Editors' Suggestion

Hard convex lens-shaped particles: Characterization of dense disordered packings

Giorgio Cinacchi*
Departamento de Física Teórica de la Materia Condensada, Instituto de Física de la Materia Condensada (IFIMAC), Instituto de Ciencias de Materiales "Nicolás Cabrera," Universidad Autónoma de Madrid, Ciudad Universitaria de Cantoblanco, E-28049 Madrid, Spain

Salvatore Torquato†
Department of Chemistry and Department of Physics, Institute for the Science and Technology of Materials, Program for Applied and Computational Mathematics, Princeton University, Princeton, New Jersey 08544, USA

(Received 3 September 2019; published 24 December 2019)

Among the family of hard convex lens-shaped particles (lenses), the one with aspect ratio equal to 2/3 is "optimal" in the sense that the maximally random jammed (MRJ) packings of such lenses achieve the highest packing fraction $\phi_{\mathrm{MRJ}} \simeq 0.73$ [G. Cinacchi and S. Torquato, Soft Matter **14**, 8205 (2018)]. This value is only a few percent lower than $\phi_{\mathrm{DKP}} = 0.762\,10\ldots$, the packing fraction of the corresponding densest-known crystalline (degenerate) packings [G. Cinacchi and S. Torquato, J. Chem. Phys. **143**, 224506 (2015)]. By exploiting the appreciably reduced propensity that a system of such optimal lenses has to positionally and orientationally order, disordered packings of them are progressively generated by a Monte Carlo method–based procedure from the dilute equilibrium isotropic fluid phase to the dense nonequilibrium MRJ state. This allows us to closely monitor how the (micro)structure of these packings changes in the process of formation of the MRJ state. The gradual changes undergone by the many structural descriptors calculated here can coherently and consistently be traced back to the gradual increase in contacts between the hard particles until the isostatic mean value of ten contact neighbors per lens is reached at the effectively hyperuniform MRJ state. Compared to the MRJ state of hard spheres, the MRJ state of such optimal lenses is denser (less porous), more disordered, and rattler-free. This set of characteristics makes them good glass formers. It is possible that this conclusion may also hold for other hard convex uniaxial particles with a correspondingly similar aspect ratio, be they oblate or prolate, and that, by using suitable biaxial variants of them, that set of characteristics might further improve.

DOI: 10.1103/PhysRevE.100.062902

I. INTRODUCTION

One defines a packing as a collection of hard (nonoverlapping) particles in a d-dimensional Euclidean ($\mathbb{R}^d$) or non-Euclidean space. Hard-particle packing problems are easy to pose but highly nontrivial to solve. Indeed, given such a collection of hard particles of a certain shape, finding the arrangements that maximize the packing fraction ϕ is a persistent discrete-geometric (optimization) problem [1–6] relevant to other sectors of mathematics as well as to science and technology. In particular, hard-particle packing problems naturally emerge whenever the subject of the investigation is a collection of many particles that mutually interact primarily via steeply repulsive interactions irrespective as to whether their typical length scale is micro- or meso- or macroscopic. They are thus pertinent to most atomic, molecular, colloidal dense multiparticle systems of interest to physics and physical chemistry [7–10], materials science [11], and physicochemical biology [12].

The simplest and most studied among the hard-particle models is the one in which the particle shape is a sphere. Depending on the specific context and interest, packings and systems of hard spheres have been extensively investigated from different perspectives and in a variety of situations: monodisperse and polydisperse, equilibrium and nonequilibrium, in Euclidean and non-Euclidean spaces across dimensions [3,4,13–18].

In the course of most of these studies, the structural characterization of the hard-sphere packings [Fig. 1(a)] has amounted to the structural characterization of the patterns of points formed by their centers [Fig. 1(b)]. This involves the calculation of suitable positional and bond-orientational correlation functions. On many other occasions, hard-sphere packings have also been viewed as two-phase media, with the hard-particle exterior constituting the matrix phase $\mathcal{V}_1$ and the complementary union of the hard-particle interiors constituting the particle phase $\mathcal{V}_2$ [Fig. 1(c)] [19]. The corresponding structural characterization involves the calculation of a sequence of positional n-point probability functions as well as a pore-size distribution function [19]. These functions can then lead to an estimate of the effective electromagnetic, mechanical, and transport properties of a heterogeneous material made of phases $\mathcal{V}_1$ and $\mathcal{V}_2$ [19].

More recently, the hard-sphere model has been extended to study dense packings and systems of hard nonspherical particles, which introduce rotational degrees of freedom [16,18]. Examples of nonspherical shapes examined include ellipsoids [20–29], spherocylinders [30–36], cutspheres [37,38], superballs [39,40], and polyhedra [41–51]. Characterizing

*giorgio.cinacchi@uam.es
†torquato@princeton.edu

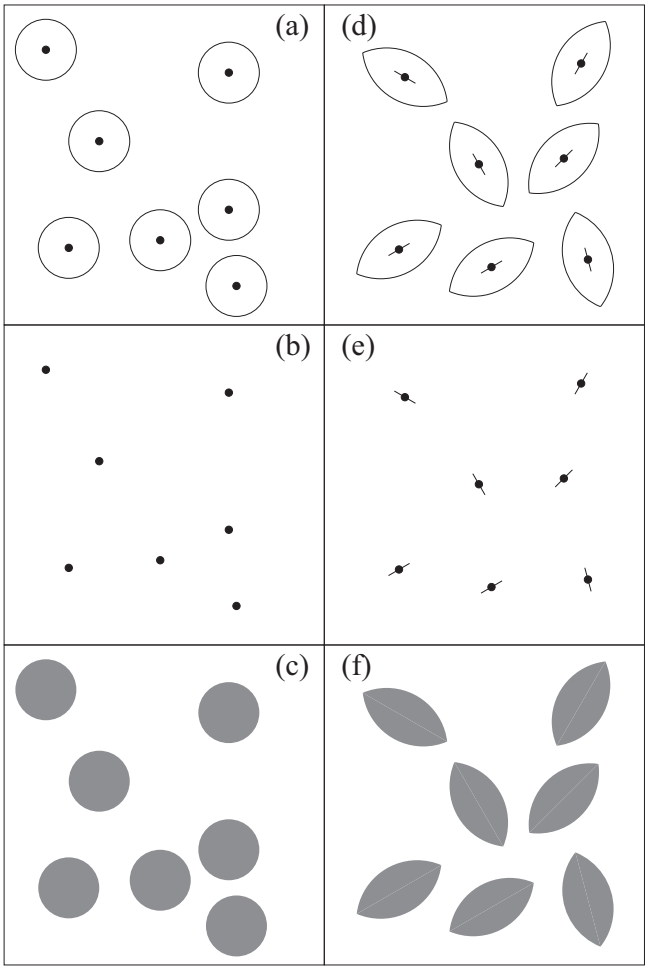

FIG. 1. Left panels: schematic illustration of a packing of hard circles (a) viewed as a pattern of points formed by the centers (b) and as a two-phase medium with the matrix phase being the white region and the particle phase being the gray region (c). Right panels: schematic illustration of a packing of hard almond-shaped particles (d) viewed as a pattern of points formed by the centroids, each one associated with a unit vector along the respective particle symmetry axis (e) and as a two-phase medium with the matrix phase being the white region and the particle phase being the gray region (f).

the structure and physical properties of equilibrium and nonequilibrium states of dense packings and systems of hard nonspherical particles continues to present many fascinating challenges [16,18].

Previously, we investigated the densest-known (crystalline) packings, equilibrium phase behavior, and nonequilibrium glassy and jammed states of hard convex lens-shaped particles (lenses) [52,53]. These hard $\mathsf{D}_{\infty\mathsf{h}}$-symmetric discoidal particles correspond to the intersection volume of two congruent three-dimensional spheres. By varying the radius of or the center-to-center distance between these spheres, the class of lenses can be generated. Each member of this class is identified by the aspect ratio $\kappa = b/a$, with a one of the infinite C_2 axes and b the C_∞ axis. The lens shape interpolates between the hard infinitesimally thin disk ($\kappa = 0$) and the hard-sphere ($\kappa = 1$) models.

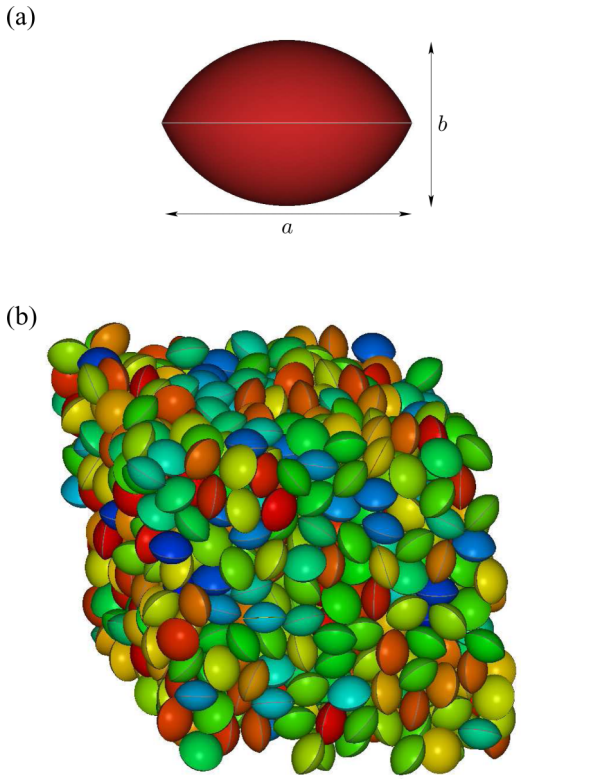

FIG. 2. (a) Image of a lens with $\kappa = b/a = 2/3$. (b) Image of a MRJ packing of lenses with $\kappa = 2/3$ with particles colored according to the angle that their C_∞ axis makes with an axis of the laboratory reference frame: the cooler the color of a particle the smaller the angle that its axis forms with that axis of the laboratory reference frame.

This work reports on the characterization of the (micro)structure of monodisperse (positionally and orientationally) disordered packings of lenses with $\kappa = 2/3$ henceforth designated as "optimal" lenses [Fig. 2(a)]. This distinguished case is designated in this manner for two intertwined reasons:

(I) Systems of optimal lenses have a substantially reduced propensity to positionally and orientationally order [53]. Disordered packings can then be generated by gently compressing from their equilibrium isotropic fluid phase up to the nonequilibrium maximally random jammed (MRJ) state [54]. This state is the one among all strictly jammed [16,18] states that minimizes suitably defined order metrics [54]. Such a gentle compression allows one to closely monitor the formation of this special hard-particle state. In addition to an extremal packing fraction ϕ_{MRJ} and an isostatic mean number of contacts per particle $\mathrm{Z} = 2d_{\mathrm{f}}$, where d_{f} is the number of degrees of freedom for a single particle [16,18], a hard-particle MRJ state has the particularly important attribute of (effective) hyperuniformity [55–58]. Hyperuniformity is a global property of a system that involves an anomalous suppression of density fluctuations at large length scales, which is completely accessible via scattering in the infinite-wavelength limit [55–58]. This unusual characteristic that special disordered systems, including hard-particle MRJ states [59–61], possess is shared with perfect crystals and quasicrystals [55–58].

(II) The MRJ state of lenses with $\kappa \simeq 2/3$ [Fig. 2(b)] is the one most densely packed: the graph of ϕ_{MRJ} versus κ has its absolute maximum at $\kappa \simeq 2/3$ [53]. This maximal value of $\phi_{\mathrm{MRJ}} \simeq 0.73$ is only $\simeq 4\%$ smaller than $\phi_{\mathrm{DKP}} = 0.762\,10\ldots$, the packing fraction of the densest-known (positionally and orientationally ordered, i.e., crystalline as well as degenerate) packings of lenses with the same value of κ [52]. It is also very close to the packing fractions reached by jammed packings of lenses with different values of κ in which positional (plastic-crystalline) or orientational (nematic liquid-crystalline) order are, however, present [53]. This fact suggests a strict interrelationship between the propensity to form (plastic- or liquid-crystalline) mesophases and the capability of reaching very dense jammed states without the need of introducing positional or orientational order [53].

In analogy with hard-sphere packings, the characterization of the (micro)structure of packings of hard nonspherical particles, such as lenses, can be simplified by viewing them as patterns of points formed by their centroids. This is, however, insufficient: the nonsphericity necessarily leads to associating the position of any centroid to a set of variables defining the orientation of the corresponding particle. In the case of $\mathsf{D}_{\infty\mathsf{h}}$-symmetric particles, such as lenses, this set is formed by the two Euler angles defining the orientation of the unit vector along the particle C_∞ axis. Thus, packings of hard $\mathsf{D}_{\infty\mathsf{h}}$-symmetric particles, such as lenses [Fig. 1(d)], can actually be viewed as patterns of points where each one is associated with a unit vector [Fig. 1(e)] rather than patterns of sole points. Consequently, their structural characterization involves not only the calculation of suitable positional and bond-orientational correlation functions, but also orientational correlation functions. Naturally, packings of hard nonspherical particles, such as lenses, can also be viewed as two-phase media [Fig. 1(f)]. Their structural characterization involves the calculation of the same sequence of n-point probability functions as well as the pore-size distribution function [19].

By calculating a number of structural descriptors, many disordered packings of optimal lenses, generated by a Monte Carlo method–based procedure from the dilute equilibrium isotropic fluid phase up to the dense nonequilibrium MRJ state, are characterized. Similarly to the hard-sphere MRJ state, the MRJ state of optimal lenses is found to be isostatic and (effectively) hyperuniform but, compared to the former, the latter is denser (less porous), more disordered, and rattler-free. Thus, even though monodisperse, optimal lenses promise to be very good (positional and orientational) glass formers.

The rest of this work consists of the following four sections: Sec. II, that lists all the quantities that have been calculated to statistically describe the (micro)structure of optimal-lens packings; Sec. III, that very briefly recalls how these optimal-lens positionally and orientationally disordered packings have been generated via a simple Monte Carlo method–based procedure; Sec. IV, that presents all the results; and Sec. V, that concludes this work.

II. LENS PACKING (MICRO)STRUCTURE CHARACTERIZATION

In the characterization of their (micro)structure, the packings were viewed either as patterns of the N lens centroids $\{\mathbf{r}_1, \ldots, \mathbf{r}_i, \ldots, \mathbf{r}_N\}$, each one associated with the respective unit vector along the lens C_∞ axis $\{\hat{\mathbf{u}}_1, \ldots, \hat{\mathbf{u}}_i, \ldots, \hat{\mathbf{u}}_N\}$, or as two-phase media with the lens exterior constituting the matrix phase $\mathcal{V}_1$ and the complementary union of the lens interiors constituting the particle phase $\mathcal{V}_2$.

A. Real-space pair-correlation functions and reciprocal-space structure factor

If lens packings are viewed as patterns of points, each one associated with a unit vector, their (micro)structure can be characterized by several real-space positional, orientational, and bond-orientational pair-correlation functions along with the reciprocal-space structure factor.

The set of real-space (real-distance) pair-correlation functions includes $g(r)$, the most basic positional pair-correlation function, proportional to the conditional probability density of finding the centroid of a lens j at a distance r from the centroid of a lens i [9,13–19], along with the orientational pair-correlation functions $\mathcal{G}_{2n}^{\hat{\mathbf{u}}\hat{\mathbf{u}}}(r)$ and the bond-orientational pair-correlation functions $\mathcal{G}_{2n}^{\hat{\mathbf{u}}\hat{\mathbf{r}}}(r)$. The latter functions are respectively defined as

$$\mathcal{G}_{2n}^{\hat{\mathbf{u}}\hat{\mathbf{u}}}(r) = \left\langle \frac{\sum_{i=1}^{N}\sum_{j\neq i}^{N} P_{2n}(\hat{\mathbf{u}}_i \cdot \hat{\mathbf{u}}_j)\delta(r - r_{ij})}{\sum_{i=1}^{N}\sum_{j\neq i}^{N}\delta(r - r_{ij})} \right\rangle \tag{1}$$

and

$$\mathcal{G}_{2n}^{\hat{\mathbf{u}}\hat{\mathbf{r}}}(r) = \left\langle \frac{\sum_{i=1}^{N}\sum_{j\neq i}^{N} P_{2n}(\hat{\mathbf{u}}_i \cdot \hat{\mathbf{r}}_{ij})\delta(r - r_{ij})}{\sum_{i=1}^{N}\sum_{j\neq i}^{N}\delta(r - r_{ij})} \right\rangle, \tag{2}$$

where $r_{ij} = |\mathbf{r}_{ij}| = |\mathbf{r}_j - \mathbf{r}_i|$, $\hat{\mathbf{r}}_{ij} = \mathbf{r}_{ij}/r_{ij}$; $\delta(r)$ is the radial Dirac δ function; $P_m(x)$ is the m-order Legendre polynomial, and angular brackets indicate an average over configurations. The $\mathcal{G}_{2n}^{\hat{\mathbf{u}}\hat{\mathbf{u}}}(r)$'s measure the degree of correlation in the orientations of two lenses whose centroids are separated by a distance r. The $\mathcal{G}_{2n}^{\hat{\mathbf{u}}\hat{\mathbf{r}}}(r)$'s measure the degree of orientational order of the fictitious "bond" $\mathbf{r}_{ij}$, established between the centroids of two lenses i and j, with respect to $\hat{\mathbf{u}}_i$.

Together with these real-space pair-correlation functions, the orientationally averaged structure factor $\mathcal{S}(k)$, essentially the Fourier transform of $h(r) = g(r) - 1$ [9,13,16,18,55,58], was also calculated. $\mathcal{S}(k)$ is defined as

$$\mathcal{S}(k) = \frac{1}{N}\left\langle \left| \sum_{j=1}^{N} \mathrm{e}^{i\mathbf{k}\cdot\mathbf{r}_j} \right|^2 \right\rangle_{\widehat{\mathbf{k}}}, \quad \mathbf{k} \neq \mathbf{0} \tag{3}$$

with $k = |\mathbf{k}|$, $\mathbf{k}$ a reciprocal-space vector and the symbol $\langle\cdot\rangle_{\widehat{\mathbf{k}}}$ indicating an average over the reciprocal-space vectors sharing the same value of k as well as over configurations. The calculation of $\mathcal{S}(k)$, made directly according to Eq. (3) rather than Fourier transforming $h(r)$, is important because its value in the limit $k \to 0$ informs one about the degree of hyperuniformity of a system. In fact, a hyperuniform many-particle system in $\mathbb{R}^d$ is one in which $\mathcal{S}(k)$ tends to zero in the limit $k \to 0$ [55–58]. Equivalently, it is one in which the local number variance associated with a spherical window of radius R, scaled by R^d, vanishes in the large-R limit [55–58].

B. Pair-correlation function of the scaled distance and contact statistics

Given the hard, convex, and nonspherical character of the particles constituting the packings, it is useful to define a positional pair-correlation function $\mathrm{g}(s)$ of the scaled distance $s_{ij} = r_{ij}/\mathrm{d}(\hat{\mathbf{r}}_{ij}, \hat{\mathbf{u}}_i, \hat{\mathbf{u}}_j)$, with $\mathrm{d}(\hat{\mathbf{r}}_{ij}, \hat{\mathbf{u}}_i, \hat{\mathbf{u}}_j)$ the distance of closest approach or contact distance between lens i and lens j. One way to define $\mathrm{g}(s)$ is to mimic the most basic physical interpretation of $g(r)$ as the ratio between the mean number of centroids found in a spherical shell of radii r and $r + dr$ centered on a given centroid and the mean number of such centroids in an isodense ideal gas (Poissonian point pattern):

$$\mathrm{g}(s) = \frac{\langle dn(s)\rangle}{\langle dn_{\mathrm{id}}(s)\rangle} = \frac{\langle dn(s)\rangle}{3\varrho\,\langle v_{\mathrm{exc}}\rangle\, s^2 ds}, \tag{4}$$

with $\langle dn(s)\rangle$ the number of centroids having a scaled distance from a central centroid $\in [s, s+ds]$ averaged over central centroids and configurations and $\langle dn_{\mathrm{id}}(s)\rangle$ the analogous mean number of centroids in an isodense ideal gas; in its turn, $\langle dn_{\mathrm{id}}(s)\rangle$ is given by $3\varrho\,\langle v_{\mathrm{exc}}\rangle\, s^2 ds$, with ϱ the number density and $\langle v_{\mathrm{exc}}\rangle$ the expected excluded volume associated with one lens completely averaged over $\hat{\mathbf{u}}_i$ and $\hat{\mathbf{u}}_j$ [62]. Differently than the full many-variable pair-correlation function $g(\mathbf{r}_{ij}, \hat{\mathbf{u}}_i, \hat{\mathbf{u}}_j)$, the positional pair-correlation function $\mathrm{g}(s)$ can be more directly compared to $g(r)$ of a hard-sphere system, $g_{\mathrm{hs}}(r)$, and its value in the $\lim_{s\to 1^+} \mathrm{g}(s) = \mathrm{g}(1^+)$ is analogously related to the pressure P of a statistically homogeneous and isotropic system:

$$\beta P = \varrho\big[1 + \tfrac{1}{2}\varrho\,\langle v_{\mathrm{exc}}\rangle\, \mathrm{g}(1^+)\big], \tag{5}$$

with $\beta = 1/(k_B T)$ and k_B the Boltzmann constant and T the absolute temperature. For a lens in a configuration, the occupancy of the bin at $s = 1$ defines the number, $\mathtt{n}_\mathrm{c}$, of lenses at contact with it. One can then calculate the probability density that a lens has $\mathtt{n}_\mathrm{c}$ contact neighbors, $\Pi(\mathtt{n}_\mathrm{c})$, along with its first moment, the mean value of $\mathtt{n}_\mathrm{c}$, as a function of ϕ, $\langle \mathtt{n}_\mathrm{c}\rangle(\phi) = \mathtt{Z}(\phi)$.

C. Lens packings as two-phase media

It is useful to view lens packings as two-phase media, in which phase 1 (matrix phase) comprises the space exterior to the particles, $\mathcal{V}_1$, and phase 2 (particle phase) comprises the space occupied by the particles, $\mathcal{V}_2$, such that $\mathcal{V}_1 \cup \mathcal{V}_2 = V \subset \mathbb{R}^3$. Their (micro)structure can then be characterized by an infinite hierarchy of n-point probability functions [19]. These functions are defined in terms of the phase indicator function:

$$I(\mathbf{x}) = \begin{cases} 0 & : \mathbf{x} \in \mathcal{V}_1 \\ 1 & : \mathbf{x} \in \mathcal{V}_2 \end{cases} \tag{6}$$

with $\mathbf{x} \in V \subset \mathbb{R}^3$ as

$$S_n(\mathbf{x}_1, ..., \mathbf{x}_n) = \langle I(\mathbf{x}_1)...I(\mathbf{x}_n)\rangle\,. \tag{7}$$

This n-point function is the probability of finding n randomly selected points at positions $\mathbf{x}_1, \ldots, \mathbf{x}_n$ in phase 2. For statistically homogeneous media, the one-point function is simply equal to the packing fraction, i.e., $S_1(\mathbf{x}) \equiv \phi$, and the two-point function depends only on the displacement vector, $S_2(\mathbf{x}_1, \mathbf{x}_2) = S_2(\mathbf{x}_2 - \mathbf{x}_1)$. If the system is also statistically isotropic, the two-point function depends only on the modulus of the distance between the two points: $S_2(\mathbf{x}_1, \mathbf{x}_2) = S_2(|\mathbf{x}_2 - \mathbf{x}_1|) = S_2(x)$. Furthermore, statistical homogeneity suffices to allow $S_2(x)$ to be separated into an "internal" component, $S_{2_{\mathrm{int}}}(x)$, that gives the probability that the two randomly selected points will be at a distance x and lie inside the same particle, and an "external" component, $S_{2_{\mathrm{ext}}}(x)$, that gives the probability that the two randomly selected points will be at a distance x and lie inside two different particles:

$$S_2(x) = S_{2_{\mathrm{int}}}(x) + S_{2_{\mathrm{ext}}}(x). \tag{8}$$

While the former component is a single-particle quantity that does not depend on ϕ except for a multiplicative factor, it is the latter component that contains information on how the (micro)structure of the packings changes with ϕ via pair correlations. Then, it is convenient to write $S_2(x)$ in terms of the positional pair-correlation functions $\Sigma_{2_{\mathrm{int}}}(x)$ and $\Sigma_{2_{\mathrm{ext}}}(x)$:

$$S_2(x) = \phi^2\left[\Sigma_{2_{\mathrm{int}}}(x) + \Sigma_{2_{\mathrm{ext}}}(x)\right]. \tag{9}$$

The one-body term $\Sigma_{2_{\mathrm{int}}}(x) = \phi^{-2} S_{2_{\mathrm{int}}}(x)$ is calculable once for each particle type and only contains information about the particle shape and size. The two-body term $\Sigma_{2_{\mathrm{ext}}}(x) = \phi^{-2} S_{2_{\mathrm{ext}}}(x)$ more importantly contains pair-correlation information. Then, it is natural to introduce the autocovariance function $\chi(x)$ [19]:

$$\chi(x) = S_2(x) - \phi^2 = \phi^2\left[\Sigma_{2_{\mathrm{int}}}(x) + \Sigma_{2_{\mathrm{ext}}}(x) - 1\right]. \tag{10}$$

The Fourier transform of $\chi(x)$ defines the spectral density $\hat{\chi}(k)$ [19], which is analogously expressible as the sum of two components, $\hat{\chi}_{\mathrm{int}}(k)$ and $\hat{\chi}_{\mathrm{ext}}(k)$:

$$\hat{\chi}(k) = \hat{\chi}_{\mathrm{int}}(k) + \hat{\chi}_{\mathrm{ext}}(k). \tag{11}$$

The internal component is given by

$$\hat{\chi}_{\mathrm{int}}(k) = \frac{\varrho}{4\pi}\int d\hat{\mathbf{k}}\,[\hat{m}(\mathbf{k})]^2\,, \tag{12}$$

where $\hat{m}(\mathbf{k})$ is the Fourier transform of the single-particle indicator function [19]

$$m(\mathbf{x}) = \begin{cases} 0 & : \mathbf{x} \notin \text{particle} \\ 1 & : \mathbf{x} \in \text{particle}. \end{cases} \tag{13}$$

The external component is given by

$$\hat{\chi}_{\mathrm{ext}}(k) = \phi^2 \frac{4\pi}{k}\int_0^\infty dx\, x\, \sin(kx)\left[\Sigma_{2_{\mathrm{ext}}}(x) - 1\right]. \tag{14}$$

In analogy with what occurs with $h(r)$ and $\mathcal{S}(k)$, knowledge of $\hat{m}(\mathbf{k})$ and $\Sigma_{2_{\mathrm{ext}}}(x)$ would allow one to calculate $\hat{\chi}(k)$ via Eqs. (11), (12), and (14). In analogy with $\mathcal{S}(k)$, $\hat{\chi}_2(k)$ was instead directly calculated using [19]

$$\hat{\chi}(k) = \frac{1}{V}\left\langle \left| \sum_{j=1}^{N} \hat{m}_j(\mathbf{k}) \mathrm{e}^{i\mathbf{k}\cdot\mathbf{r}_j} \right|^2 \right\rangle_{\widehat{\mathbf{k}}}, \quad \mathbf{k} \neq \mathbf{0}. \tag{15}$$

The calculation of $\hat{\chi}(k)$ is important because its value in the limit $k \to 0$ informs one about the degree of hyperuniformity for a two-phase medium. In fact, a hyperuniform two-phase system in $\mathbb{R}^d$ is one in which $\hat{\chi}(k)$ tends to zero in the limit $k \to 0$ [56–58]. Equivalently, it is one in which the local volume fraction variance associated with a spherical

window of radius R, scaled by R^d, vanishes in the large-R limit [56–58]. One should note that, in a monodisperse system of hard (non)spherical particles, the behavior of $\mathcal{S}(k)$ and that of $\hat{\chi}(k)$ in the limit $k \to 0$ are interconnected [57] such that the two types of hyperuniformity, that of a point pattern and that of a two-phase medium, are either both absent or both present.

One additional important quantity that characterizes a two-phase medium is the pore-size distribution function $\mathcal{P}(\delta)$ together with its first, $\langle\delta\rangle$, and second, $\langle\delta^2\rangle$, moments. Here, δ is the maximal radius of a hard sphere, whose center is a random point in the $\mathcal{V}_1$ phase, that is completely insertable into this phase [19].

The quantities $S_2(x)$, $\langle\delta\rangle$, and $\langle\delta^2\rangle$ can lead to an estimate of the effective electromagnetic, mechanical, and transport properties of a random heterogeneous material made of phases $\mathcal{V}_1$ and $\mathcal{V}_2$ [19].

III. LENS PACKING GENERATION

Due to the appreciably reduced propensity of optimal lenses to positionally and orientationally order [53], packings of $N = 1013$ of them, each with a surface area $S = 2\sigma^2$, with σ the unit of length, were progressively generated by gently compressing the low-density equilibrium isotropic fluid phase until reaching the high-density nonequilibrium MRJ state. This compression was carried out via an isobaric(-isothermal) Monte Carlo method–based procedure using a triclinic computational box of volume V and variable shape and size, and periodic boundary conditions [63]. This allowed us to closely monitor how the (micro)structure of these packings changes in the process of formation of the MRJ state.

IV. RESULTS

One very important attribute of any hard-particle packing is its packing fraction $\phi = \varrho v = N/Vv$, where v is the particle volume. The change in ϕ as a dilute equilibrium isotropic fluid system of optimal lenses is gently compressed until reaching the dense nonequilibrium MRJ state is shown in Fig. 3. In this figure, the inverse compressibility factor, $\frac{\varrho}{\beta P}$, is plotted as a function of ϕ. The monotonic gentle descent of $\frac{\varrho}{\beta P}$ bends further downwards at $\phi \approx 0.65$. Then, it continues essentially linearly, in accordance to free-volume theory (fvt) [64], until the MRJ state is reached at the fvt-extrapolated value $\phi_{\rm MRJ} \simeq 0.73$. This bend is particularly well appreciated by comparing the numerical simulation data to a past analytic equation of state proposed for the isotropic fluid phase of monodisperse systems of hard convex nonspherical particles [65]:

$$\frac{\beta P}{\varrho} = \frac{1}{1-\phi} + \frac{3\alpha\phi}{(1-\phi)^2} + \frac{3\alpha^2\phi^2 - \alpha(6\alpha-5)\phi^3}{(1-\phi)^3}, \quad (16)$$

where $\alpha = \bar{R}S/(3v)$ is a nonsphericity parameter written in terms of the mean curvature radius $\bar{R}$, S, and v. This analytic equation of state works very well within the equilibrium fluid and the metastable fluid states but, doomed by the unphysical pole at $\phi = 1$, significantly departs from the numerical simulation data in the glassy and MRJ states. The value of $\phi_{\rm MRJ} \simeq 0.73$ is only 4% smaller than the value of $\phi_{\rm DKP} = 0.76210\ldots$ [52]. For a given dimensionality d of the Euclidean space,

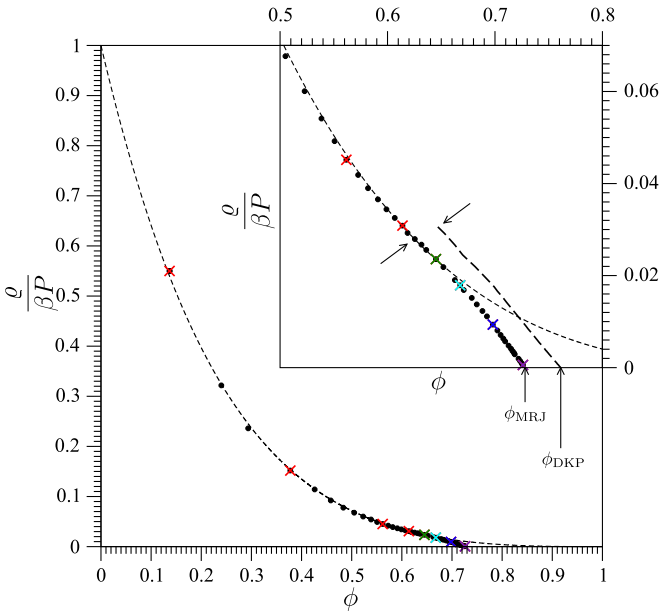

FIG. 3. Inverse compressibility factor $\frac{\varrho}{\beta P}$ as a function of packing fraction ϕ (black circles). Those marked with a colored cross are the state points at which a detailed analysis of the (micro)structure was carried out. These state points are representative of the equilibrium fluid (red), metastable fluid (green), glassy (cyan and blue), and MRJ (indigo) states. The short-dashed curve is the analytic equation of state of Eq. (16). The inset focuses on the high-ϕ regime where the high-ϕ equation of state for the equilibrium crystal is also included as a long-dashed curve and the two diagonal arrows indicate isotropic fluid–crystalline solid coexistence [52] while the two vertical arrows indicate the values of ϕ for, respectively, the maximally random jammed (MRJ) state and the densest-known packings (DKP) [52].

the closer the value of the ratio $\phi_{\rm MRJ}/\phi_{\rm DKP}$ is to unity the greater the propensity of a monodisperse system of hard particles is to form mechanically stable glassy states. The equilibrium crystal equation of state starts from the value of $\phi_{\rm DKP}$ [52]. The corresponding $\frac{\varrho}{\beta P}$ behaves essentially linearly as a function of ϕ, in accordance to fvt [64]. Its slope is similar to that of $\frac{\varrho}{\beta P}$ versus ϕ in the nonequilibrium glassy state.

In the following sections, the (micro)structure of packings representative of the equilibrium fluid, metastable fluid, glassy and MRJ states are characterized via the structural descriptors from Sec. II.

A. Real-space pair-correlation functions and reciprocal-space structure factor

The positional pair-correlation function $g(r)$ is the most basic function that describes the (micro)structure of a statistically homogeneous and isotropic system [8,9,13–19]. This function is given in Fig. 4 at several values of ϕ from the dense equilibrium fluid phase to the nonequilibrium MRJ state. These $g(r)$'s have the form that this function typically takes on in the dense fluid state of a system composed of hard moderately nonspherical particles. The positional disordered character of the system is revealed, globally, by the fast damped-exponential peak decay and valley rise towards the long-distance limit value of unity. In addition, the

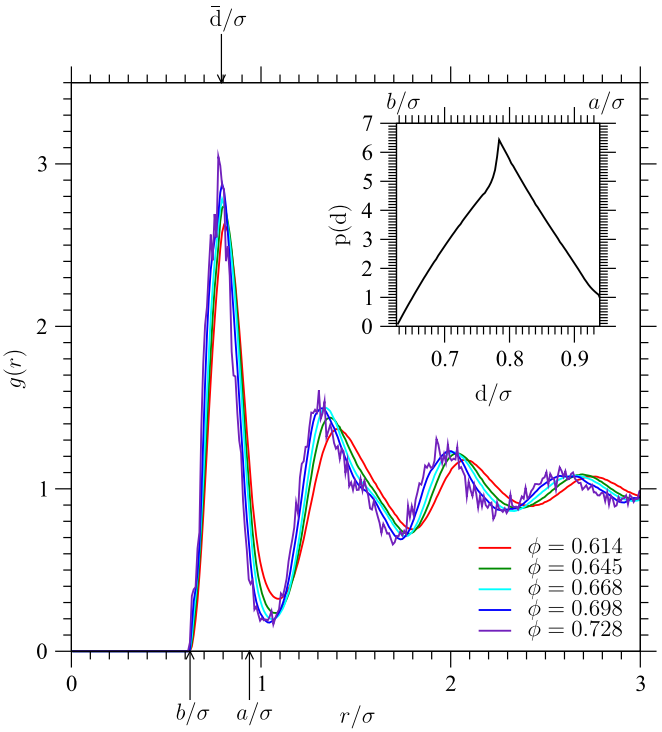

FIG. 4. Pair-correlation function $g(r)$ at several values of packing fraction ϕ representative of the equilibrium fluid (red), metastable fluid (green), glassy (cyan and blue), and MRJ (indigo) states. The arrows indicate the value of a, one of the optimal-lens C_2 axes; b, the optimal-lens C_∞ axis; and $\bar{\mathrm{d}}$, the *in vacuo* mean contact distance. The inset shows the optimal-lens *in vacuo* probability density function of the contact distance p(d), i.e., the probability density to find two randomly chosen optimal lenses whose contact distance $\in [\mathrm{d}, \mathrm{d} + d\mathrm{d}]$.

principal peak abscissa value remains essentially stuck at $\simeq \bar{\mathrm{d}} = \int_b^a \mathrm{dp(d)}d\mathrm{d} = 0.791\ldots\sigma$, the value of the *in vacuo* mean contact distance (main and inset panels of Fig. 4). This fact suggests that these hard particles, even locally, do not generally have a preferred positional organization. The principal peak abscissa value is moderately, yet perceptibly, moving towards the value of the *in vacuo* most probable contact distance, $0.784\ldots\sigma$ (inset of Fig. 4), as ϕ increases, which causes more contacts to be established between the hard particles. The successive peaks shift towards the principal peak while the principal valley deepens as ϕ increases. During this compression, there is no evident sign of the system becoming glassy except, in retrospect, the moderate displacement of the principal peak abscissa value, the appearance of a tenuous shoulder at $r \approx 1.5\sigma$ and, especially, the progressive roughness of the curve. This roughness is a direct consequence of the rigidity that the system is acquiring and that its relatively small size makes noticeable [66]. The form of $g(r)$ for a system of optimal lenses in a disordered state differs from that of a system of hard spheres in a disordered state. They differ not just in the principal peak shape but especially in their overall smoothness as the MRJ state is approached. Due to the nonsphericity of the hard particles, the principal peak is rounded off rather than cusped. It is reminiscent of $g(r)$ of a monodisperse system of soft (attractive-repulsive) spherical (e.g., Lennard-Jones) particles in its liquid phase [9,13]. Due again to the nonsphericity of the hard particles, the form of this function does not show any singularity or a split second peak, both features of the hard-sphere MRJ state $g(r)$ [16,18].

Directly connected to $g(r)$ is the (orientationally averaged) structure factor $\mathcal{S}(k)$. The overall form of $\mathcal{S}(k)$, particularly its limit value of unity as $k \to \infty$, at values of ϕ in the dense equilibrium fluid, nonequilibrium glassy and MRJ states confirms the positionally disordered character of all these states (Fig. 5). The strong similarity among all these curves indicates that these states are cognate with one another (Fig. 5). In parallel to what is observed for $g(r)$ (Fig. 4), the progressive roughness of the curve as ϕ increases (Fig. 5) is a reflection of the progressive rigidity that the system is acquiring and that the small size of the system makes noticeable [66]. In the equilibrium fluid state, the value of $\mathcal{S}(0) > 0$ obtained by quadratically fitting the low-k $\mathcal{S}(k)$ data matches the value obtained from the isothermal compressibility [Fig. 5(a)], which, in equilibrium, is known to be related to $\mathcal{S}(0)$ [9]. In the denser nonequilibrium states, the extrapolated value of $\mathcal{S}(0)$ keeps progressively decreasing [Figs. 5(b) and 5(c)]. With the caveat that the present system size is not so large to allow for very small values of k to be investigated and the statistics of $\mathcal{S}(k)$ at these very small k's to be extremely good, one may conclude that the values that $\mathcal{S}(k)$ takes on as $k \to 0$ are so small [Fig. 5(c)] that the system becomes effectively hyperuniform on approaching the MRJ state: in the neighborhood of $k = 0$, $\mathcal{S} \simeq 10^{-3}$ while $\mathcal{S} \simeq 4$ at its principal peak [58].

The nonsphericity of the present hard particles offers the possibility to define and evaluate new, orientational, pair-correlation functions as well as more precise bond-orientational pair-correlation functions. Given the cylindrically symmetric character of the present hard particles, $\mathcal{G}_2^{\hat{\mathbf{u}}\hat{\mathbf{u}}}(r)$ and $\mathcal{G}_2^{\hat{\mathbf{u}}\hat{\mathbf{r}}}(r)$ are the most basic orientational and bond-orientational pair-correlation functions. Their form at several values of ϕ, from the moderately dense equilibrium fluid to the dense nonequilibrium MRJ states, are shown in Figs. 6 and 7. The vanishing of $\mathcal{G}_2^{\hat{\mathbf{u}}\hat{\mathbf{u}}}(r)$ and $\mathcal{G}_2^{\hat{\mathbf{u}}\hat{\mathbf{r}}}(r)$ as $r \to \infty$ demonstrates the globally orientationally disordered character of all considered packings. In each panel of these figures, $\mathcal{G}_2^{\hat{\mathbf{u}}\hat{\mathbf{u}}}(r)$ and $\mathcal{G}_2^{\hat{\mathbf{u}}\hat{\mathbf{r}}}(r)$ are compared to two functions. The first is the limit form that $\mathcal{G}_2^{\hat{\mathbf{u}}\hat{\mathbf{u}}}(r)$ and $\mathcal{G}_2^{\hat{\mathbf{u}}\hat{\mathbf{r}}}(r)$ respectively take on as $\phi \to 0$. This corresponds to a calculation where two particles are taken at a fixed centroid distance r and whose orientations are completely random except that the nonoverlap constraint has to be complied with. The domain of these functions is $[b, \infty)$. The second is the limit form that $\mathcal{G}_2^{\hat{\mathbf{u}}\hat{\mathbf{u}}}(r)$ and $\mathcal{G}_2^{\hat{\mathbf{u}}\hat{\mathbf{r}}}(r)$ respectively take on in a calculation where two particles are taken whose orientations are completely random except that the particles are constrained to touch. They are related to the form respectively taken on by $\mathcal{G}_2^{\hat{\mathbf{u}}\hat{\mathbf{u}}}(r)$ and $\mathcal{G}_2^{\hat{\mathbf{u}}\hat{\mathbf{r}}}(r)$ as the MRJ state is approached. The domain of these functions is $[b, a]$. One can observe that $\mathcal{G}_2^{\hat{\mathbf{u}}\hat{\mathbf{u}}}(r)$ and $\mathcal{G}_2^{\hat{\mathbf{u}}\hat{\mathbf{r}}}(r)$ progressively pass from the respective first limit form and change so as to "adhere" to the respective second limit form as ϕ increases. Even in the dense packings, the second limit form cannot be completely "adhered" to since, in general, the latter form is the result of a purely two-body calculation and, in particular for sufficiently large r, not all pairs of particles whose centroids

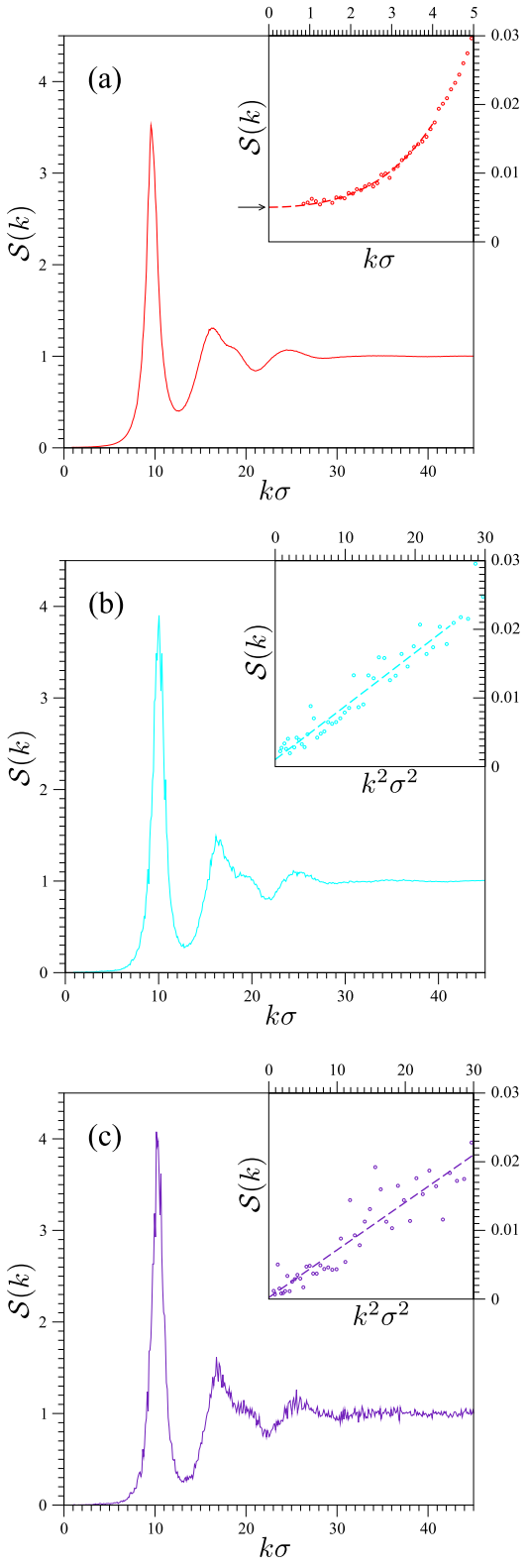

FIG. 5. Orientationally averaged structure factor $\mathcal{S}(k)$ at several values of packing fraction ϕ: (a) equilibrium fluid at $\phi = 0.614$; (b) glassy state at $\phi = 0.668$; (c) MRJ state at $\phi = 0.728$. In any panel, the top-right inset focuses on the low-k regime with the dashed curve being a quadratic fit. In (a) the arrow marks the value of $\mathcal{S}(0)$ obtained from the isothermal compressibility; in (b) and (c) it had better plot $\mathcal{S}(k)$ as a function of k^2 so as to more clearly show its diminishing trend as $k \to 0$.

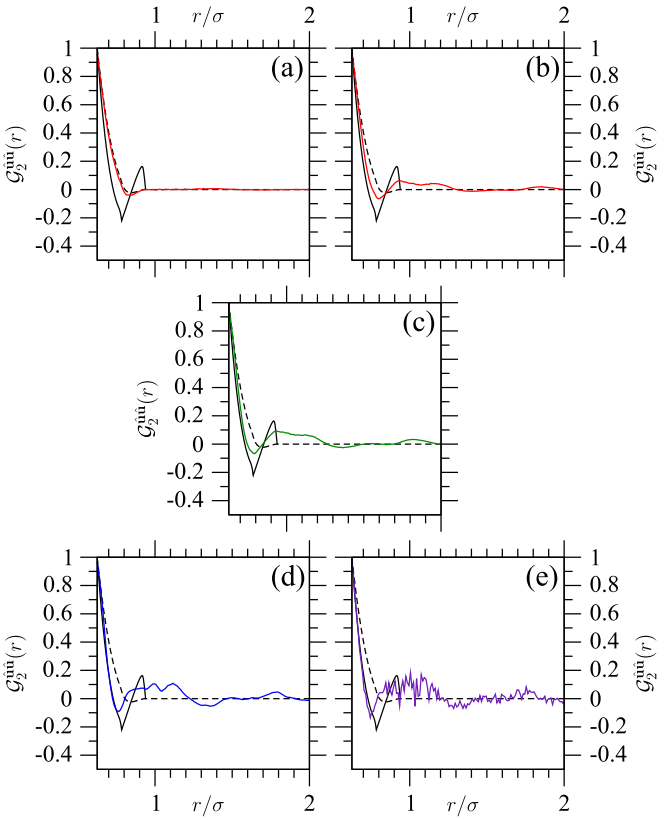

FIG. 6. Pair-correlation function $\mathcal{G}_2^{\hat{\mathbf{u}}\hat{\mathbf{u}}}(r)$ at several values of packing fraction ϕ representative of the equilibrium fluid [(a) $\phi = 0.378$; (b) $\phi = 0.614$], metastable fluid [(c) $\phi = 0.645$], glassy [(d) $\phi = 0.698$], and MRJ [(e) $\phi = 0.728$] states. In each panel, the black curves correspond to the limit forms this function takes on when calculated considering two randomly chosen lenses either free (dashed) or touching (continuous).

are separated by r are necessarily touching. Nonetheless, the second limit form sets a paragon stone by which to understand how $\mathcal{G}_2^{\hat{\mathbf{u}}\hat{\mathbf{u}}}(r)$ and $\mathcal{G}_2^{\hat{\mathbf{u}}\hat{\mathbf{r}}}(r)$ changes as ϕ increases. The fact that $\mathcal{G}_2^{\hat{\mathbf{u}}\hat{\mathbf{u}}}(r)$ and $\mathcal{G}_2^{\hat{\mathbf{u}}\hat{\mathbf{r}}}(r)$ are taking on a form that closely resembles the respective second limit form is an indication that the packings are also locally orientationally disordered. Even when only viewing $\mathcal{G}_2^{\hat{\mathbf{u}}\hat{\mathbf{u}}}(r)$ and $\mathcal{G}_2^{\hat{\mathbf{u}}\hat{\mathbf{r}}}(r)$, the process of formation of the nonequilibrium MRJ state from the equilibrium fluid state is one in which the salient features of the (micro)structure "exasperate" quantitatively, as the degree of contactedness between the particles *a fortiori* increases, without, however, significantly changing qualitatively.

B. Pair-correlation function of the scaled distance and contact statistics

The moderate nonsphericity of the present hard particles is responsible for $g(r)$ having a form resembling more that of liquid argon [9,13] rather than that of the hard-sphere fluid [9,13–19]. Considering the scaled distance $s = r/\mathrm{d}(\hat{\mathbf{r}}_{ij}, \hat{\mathbf{u}}_i, \hat{\mathbf{u}}_j)$ instead of the real distance r restores a pair-correlation function $\mathrm{g}(s)$ with a "hard-sphere-fluid–like" form (Fig. 8). By construction, as $\phi \to 0$, $\mathrm{g}(s)$ is guaranteed to approach the corresponding unit-diameter hard-sphere fluid $g(r)$, $g_{\mathrm{hs}}(r)$,

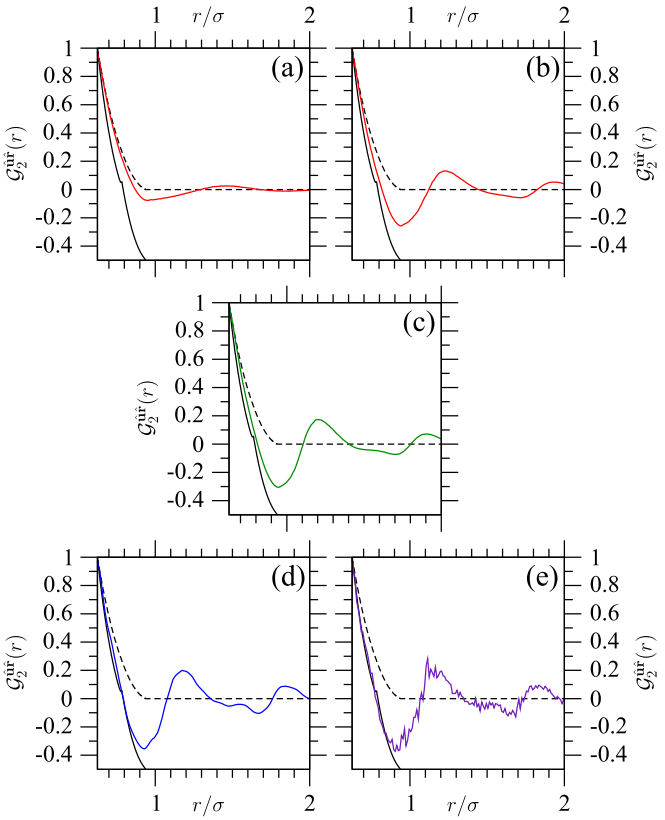

FIG. 7. Pair-correlation function $\mathcal{G}_2^{\hat{u}\hat{r}}(r)$ at several values of packing fraction ϕ representative of the equilibrium fluid [(a) $\phi = 0.378$; (b) $\phi = 0.614$], metastable fluid [(c) $\phi = 0.645$], glassy [(d) $\phi = 0.698$], and MRJ [(e) $\phi = 0.728$] states. In each panel, the black curves correspond to the limit forms this function takes on when calculated considering two randomly chosen lenses either free (dashed) or touching (continuous).

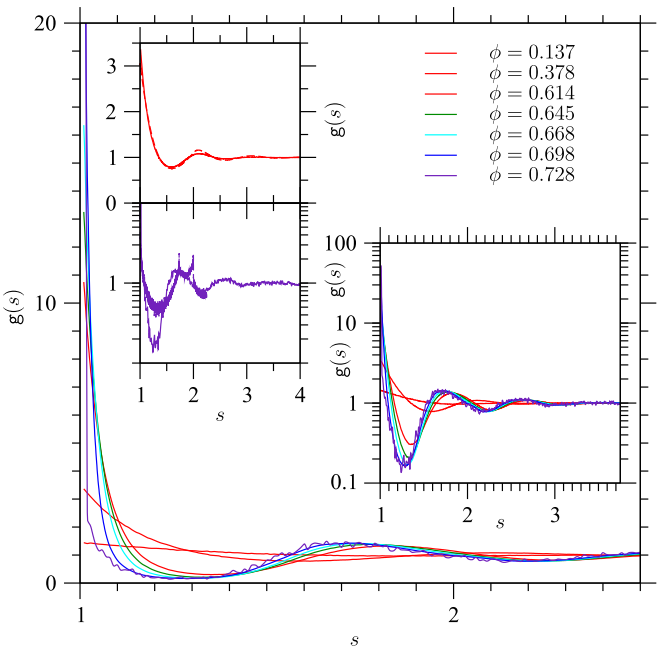

FIG. 8. Pair-correlation function $\mathrm{g}(s)$ of the scaled distance s, obtained by dividing the distance r separating two lens centroids by the appropriate contact distance, at several values of packing fraction ϕ representative of the equilibrium fluid (red), metastable fluid (green), glassy (cyan and blue), and MRJ (indigo) states. The top-left inset shows $\mathrm{g}(s)$ in the moderately dense equilibrium fluid phase at $\phi = 0.378$ (continuous curve) compared to the Percus-Yevick approximation result for the $g(r)$ of the hard-sphere fluid at the same value of ϕ (dashed curve). The bottom-left inset shows $\mathrm{g}(s)$ at the MRJ state (continuous thinner curve) compared to the $g(r)$ of the hard-sphere MRJ state (dashed thicker curve) with the ordinate axis on a logarithmic scale. The bottom-right inset shows the same $\mathrm{g}(s)$'s as the main panel but with the ordinate axis on a logarithmic scale.

i.e., the step function

$$\Theta(r) = \begin{cases} 0: & 0 \leqslant r \leqslant 1 \\ 1: & r > 1. \end{cases} \tag{17}$$

It becomes of interest to investigate how $\mathrm{g}(s)$ compares to $g_{\mathrm{hs}}(r)$ as ϕ increases. This may be done by using, for the hard-sphere positional pair-correlation function, the Percus-Yevick (PY) approximation, $g_{\mathrm{hs}}^{\mathrm{PY}}(r)$, known to be good throughout the hard-sphere equilibrium fluid phase [9,13,14,17]. Indeed, $g_{\mathrm{hs}}^{\mathrm{PY}}(r)$ compares well to $\mathrm{g}(s)$ up to moderate values of ϕ (top-left inset of Fig. 8). However, the two positional pair-correlation functions progressively depart from one another as ϕ increases and surpasses $\phi_{\mathrm{hs,frz}} = 0.494$, the value of ϕ at which the hard-sphere fluid freezes [9,13–18]. Beyond $\phi_{\mathrm{hs,frz}}$, the PY approximation quickly deteriorates to such an extent that, in the proximity of $\phi_{\mathrm{hs,MRJ}} \simeq 0.64$, the value of ϕ at the hard-sphere MRJ state [54], $g_{\mathrm{hs}}^{\mathrm{PY}}(r)$ displays unphysically negative values. The "true" $g_{\mathrm{hs}}(r)$ progressively loses a fluidlike appearance to finally assume the characteristic form with a singular split second peak that it exhibits at the MRJ state (bottom-left inset of Fig. 8) [16,18]. On the contrary, $\mathrm{g}(s)$ smoothly changes as ϕ increases towards ϕ_{MRJ}, always maintaining a hard-sphere-fluid–like form (Fig. 8). Indeed, $\mathrm{g}(s)$ is tending to acquire an approximate "delta-plus-step-with-a-gap" form rather than the form characteristic of the three-dimensional hard-sphere MRJ state (Fig. 8). This is an example of the decorrelation principle that is acting as d_{f} increases either because the dimensionality d of the Euclidean space increases [67] and/or rotational degrees of freedom are added. One can compare the abscissa value of the minimum of $\mathrm{g}(s)$ at the MRJ state, $s \approx 1.3$ (Fig. 8), with the optimal value of the gap parameter σ^* discussed in the analysis of three- and higher-dimensional disordered hard-sphere systems aimed at estimating the scaling of ϕ_{MRJ} as $d \to \infty$ [67].

The numerical calculation of $\mathrm{g}(s)$ [Eq. (4) and Fig. 8] leads to the estimate of the number of neighboring particles that are in contact with a central particle. In fact, this number, $\mathtt{n}_{\mathtt{c}}$, is here defined as the number of particles whose $s \in [1, 1 + ds]$ with $ds = 0.01$. By averaging over central particles and configurations, one can calculate the probability, $\Pi(\mathtt{n}_{\mathtt{c}})$, that a particle has $\mathtt{n}_{\mathtt{c}}$ contact neighbors. The histograms of $\Pi(\mathtt{n}_{\mathtt{c}})$ at several values of ϕ from the dense equilibrium fluid to the nonequilibrium MRJ states are shown in Fig. 9. During this compression, besides the expected progressive increase of the mean value of $\mathtt{n}_{\mathtt{c}}$, $\langle \mathtt{n}_{\mathtt{c}} \rangle = \mathtt{Z}$ (Fig. 10) [68], and that of the most probable value of $\mathtt{n}_{\mathtt{c}}$, the form of the histograms passes from being left- to right-skewed. This fact decisively

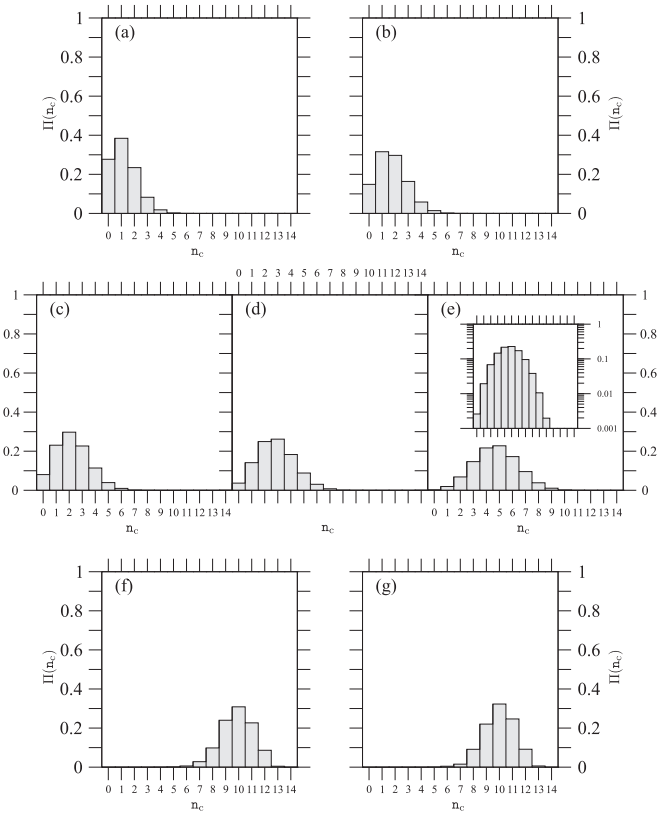

FIG. 9. Contact neighbor number probability $\Pi(n_c)$ at several values of packing fraction ϕ representative of the equilibrium fluid [(a) $\phi = 0.562$; (b) $\phi = 0.614$], metastable fluid [(c) $\phi = 0.645$], glassy [(d) $\phi = 0.668$; (e) $\phi = 0.698$], and (quasi)MRJ states [(f) $\phi = 0.726$; (g) $\phi = 0.728$]. In (e), the inset reproduces the main panel with the ordinate axis on a logarithm scale.

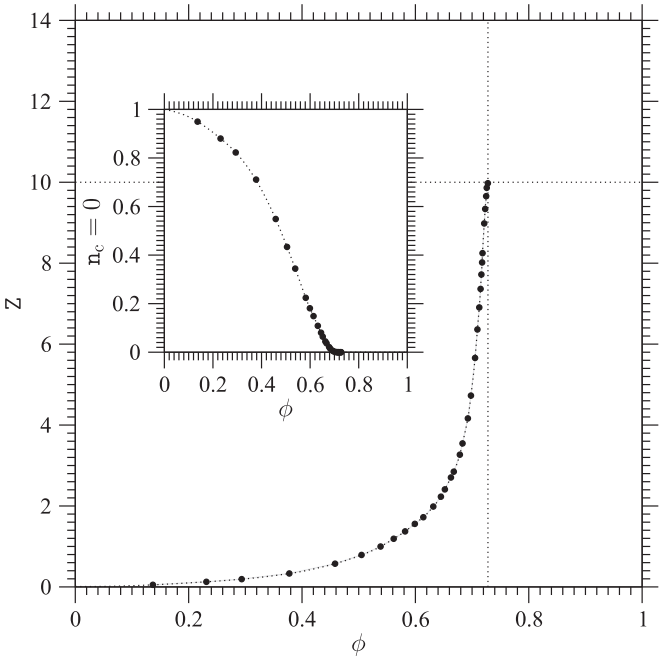

FIG. 10. Mean contact neighbor number Z as a function of packing fraction ϕ (black circles and eye-guide dotted curve); the horizontal and vertical dotted lines intercept at (ϕ_{MRJ},10). The inset shows the number of "rattlers", $n_c = 0$, as a function of packing fraction ϕ (black circles and eye-guide dotted curve).

contributes to the upswing of Z in the proximity of the MRJ state until it reaches the isostatic mean value of 10 at the MRJ state (Fig. 10). During this compression, the number of "rattlers," i.e., the particles with no contact neighbors, $n_c = 0$, quickly diminishes and vanishes in close proximity of the MRJ state (Figs. 9 and 10). This occurs at the setting in of fully glassy behavior, in turn corresponding to the setting in of a fvt-like linear behavior of $\varrho/\beta P$ versus ϕ (Fig. 3). The number of "rattling" optimal lenses is rather large at values of $\phi \simeq \phi_{hs,MRJ} \simeq 0.64$ [54]. This is consistent with the capability of a system of optimal lenses to form an equilibrium fluid denser than the densest hard-sphere equilibrium fluid at $\phi_{hs,frz}$. It is also consistent with the capability of a system of optimal lenses to reach a MRJ state not only $\simeq$14% denser than the hard-sphere MRJ state but also remarkably devoid of any rattler. Thus far, no procedure has been able to generate a rattler-free three-dimensional hard-sphere MRJ state [16,18,58].

C. Lens packings as two-phase media

1. Two-point correlation function and spectral density

The most important component of the two-point probability function $S_2(x)$ is the external pair-correlation function $\Sigma_{2ext}(x)$. This function is proportional to the conditional probability to find the two points at a distance x and inside two different particles (Fig. 11). Irrespective of the value of ϕ, this function rather quickly reaches its $x \to \infty$ limit

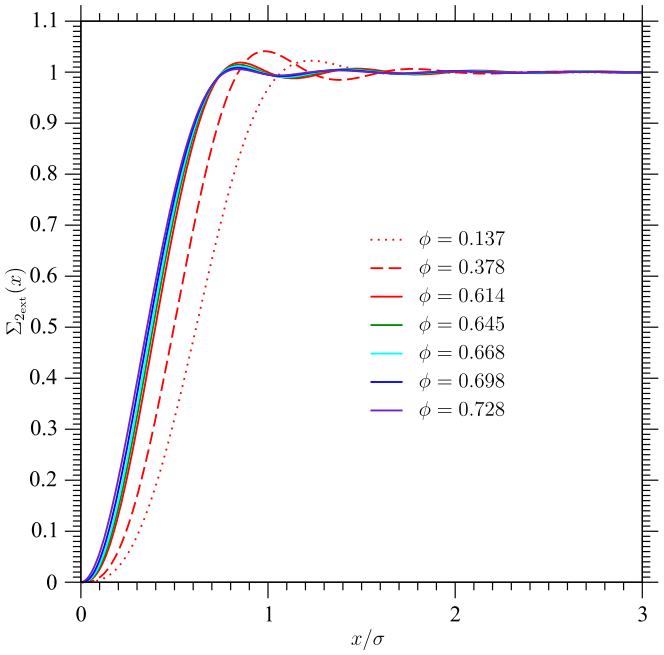

FIG. 11. The external part of the two-point correlation function $\Sigma_{2ext}(x)$ at several values of packing fraction ϕ representative of the equilibrium fluid (red: dotted, dashed, and continuous), metastable fluid (green), glassy (cyan and blue), and MRJ (indigo) states.

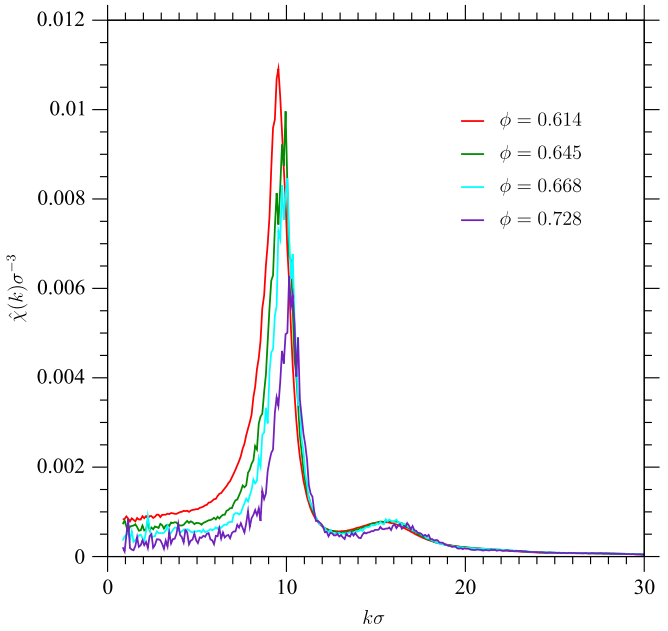

FIG. 12. Spectral density $\hat{\chi}(k)$ at several values of packing fraction ϕ representative of the equilibrium fluid (red), metastable fluid (green), glassy (cyan), and MRJ (indigo) states.

value of unity. On increasing ϕ, $\Sigma_{2\text{ext}}(x)$ is expectedly progressively "pushed" towards $x = 0$ while growing damped oscillations are developed. They show the largest amplitude in the moderately dense equilibrium fluid phase. Then, these damped oscillations progressively fade away as ϕ approaches the value corresponding to the equilibrium fluid phase at freezing. From this point, on further increasing ϕ, $\Sigma_{2\text{ext}}(x)$ moderately changes its form: it keeps being pushed mildly towards $x = 0$ and reduces its damped oscillations. This is diametrically opposed to what happens to $g(r)$ whose damped oscillations increase with ϕ. This suggests that an analytic theory that reliably extrapolates $\Sigma_{2\text{ext}}(x)$ to $x \to \infty$ might be more feasible than an analogous analytic theory for $g(r)$. That analytic theory would allow one to calculate $\hat{\chi}(k)$ by Fourier transform even for $k \to 0$. Short of such an analytic theory, $\hat{\chi}(k)$ has directly been calculated (Fig. 12). Leaving aside the expected progressive lowering of the curve as ϕ increases, consistent with the progressive decrease of $\mathcal{S}(k)$ at small values of k (Fig. 5), the overall form of $\hat{\chi}(k)$ changes little as the system goes from the equilibrium fluid to the nonequilibrium MRJ states.

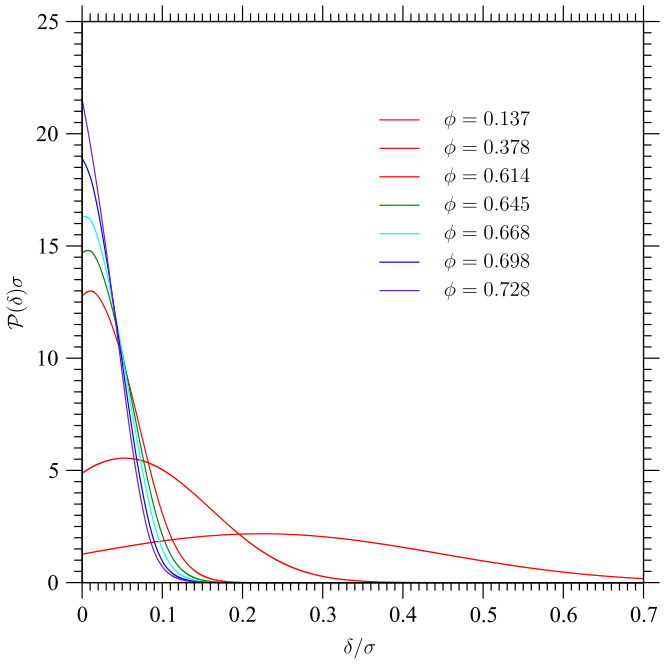

FIG. 13. Pore-size distribution function $\mathcal{P}(\delta)$ at several values of packing fraction ϕ, from the low-ϕ equilibrium fluid to the high-ϕ MRJ states. Red curves correspond to the equilibrium fluid state; the green curve corresponds to the metastable fluid state; the cyan and blue curves correspond to the glassy state; the indigo curve corresponds to the MRJ state.

2. *Pore-size statistics*

One additional important quantity when characterizing a two-phase medium is its pore-size distribution function $\mathcal{P}(\delta)$ (Fig. 13). Its form significantly changes when going from the dilute equilibrium fluid to the dense nonequilibrium MRJ

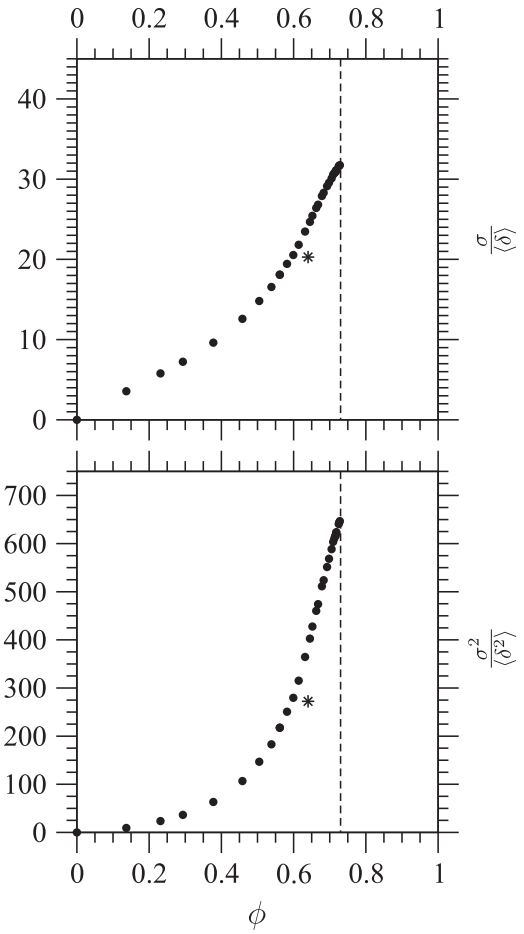

FIG. 14. Inverse of mean pore size $\langle\delta\rangle$ and mean-square pore size $\langle\delta^2\rangle$ as a function of packing fraction ϕ. The vertical dashed lines mark the value of ϕ of the optimal-lens MRJ state. The asterisks are the corresponding data for the hard-sphere MRJ state.

states. In addition to the expected progressive sharpening and shifting of this function upward as δ tends to zero, $\mathcal{P}(\delta = 0)$ is its maximal value and (consequently) its derivative at $\delta = 0$ changes from positive to negative at sufficiently high ϕ. This occurs in correspondence to the system becoming glassy and then reaching the MRJ state. Either directly or from $\mathcal{P}(\delta)$, one can calculate the first two moments of this distribution function, $\langle\delta\rangle$ and $\langle\delta^2\rangle$ (Fig. 14). It proved important to report the inverse of these two quantities versus ϕ so as to reveal the quasisigmoidal form that these two curves have on approaching the MRJ state. This allows one to appreciate how the graph of ϕ versus $1/\langle\delta\rangle$ and that of ϕ versus $1/\langle\delta^2\rangle$ mirror the graph of $\varrho/\beta P$ versus ϕ (Fig. 3): the bend that these former curves have at $\phi \approx 0.65$ parallels the bend that this latter curve has at the same value of ϕ. For the hard-sphere MRJ state at $\phi_{\mathrm{hs,MRJ}} \simeq 0.64$, $\langle\delta\rangle \simeq 0.063D$ and $\langle\delta^2\rangle \simeq 0.006D^2$, with D the hard-sphere diameter [69]. The latter length is presently assimilable to $\bar{\mathrm{d}}$. Thus, for the hard-sphere MRJ state at $\phi_{\mathrm{hs,MRJ}} \simeq 0.64$, $\langle\delta\rangle \simeq 0.049\sigma$ and $\langle\delta^2\rangle \simeq 0.0037\sigma^2$. These values are significantly larger than the respective value for optimal lenses at the same value of $\phi \simeq 0.64$: another confirmation that optimal lenses are better (ordered and disordered) packers than hard spheres.

V. CONCLUSIONS

In the class of hard convex lens-shaped particles, the member with aspect ratio equal to $2/3$ is optimal in the sense that its maximally random jammed state is the densest, which imparts them with a reduced propensity to positionally and/or orientationally order on compressing from the equilibrium isotropic fluid. This makes them a suitable hard nonspherical particle model to carefully investigate the process of formation of the maximally random jammed state without interference from not only full but also partial, plastic or liquid, crystallization while keeping the system monodisperse. Thus, by using a simple Monte Carlo method–based procedure, monodisperse packings of such hard nonspherical particles are generated by compressing the equilibrium isotropic fluid until reaching the nonequilibrium maximally random jammed state.

To characterize how the (micro)structure of these packings changes in this process, many structural descriptors are calculated. These structural descriptors undergo gradual, quantitative but not qualitative, changes: the compression "exasperates" features that are already present in the dense equilibrium isotropic fluid. These changes can coherently and consistently be traced back to the gradual increase of contacts between these hard particles on densification until the isostatic mean value of ten contact neighbors per particle is reached at the effectively hyperuniform maximally random jammed state. Even the bend in the inverse compressibility factor versus packing fraction curve, a macroscopic signature of glass formation, can be traced back to the pore-size distribution function assuming its absolute maximum at a pore size equal to zero.

The analysis of contact statistics can be seen as part of the calculation of the pair-correlation function of the scaled distance obtained by dividing the real distance by the orientation-dependent contact distance. The form of this special pair-correlation function compares well to that of a hard-sphere fluid up to moderate values of packing fraction. For values of the packing fraction approaching and surpassing the value at hard-sphere freezing, the two pair-correlation functions depart more and more from one another. The hard-sphere pair-correlation function is known to acquire a form distinct from that in the equilibrium fluid, with a singular split second peak, as the maximally random jammed state is approached and finally reached. Instead, the pair-correlation function of the scaled distance always maintains a fluidlike form that approximates a delta-plus-step-with-a-gap form as the maximally random jammed state is approached and finally reached. This can be seen as an example of the decorrelation principle acting as the number of degrees of freedom increases.

Compared to the hard-sphere maximally random jammed state, the maximally random jammed state of the present hard nonspherical particles is not only denser but also has a packing fraction only a few percent smaller than the packing fraction of the corresponding densest-known crystalline (degenerate) packings. Based on the decorrelation principle, it can be considered more disordered. In addition, it is less porous and rattler-free. These characteristics make it a significantly better glassy material and the investigation of its effective electromagnetic, mechanical, and trasport properties [19,70] opportune.

It is possible that other hard convex uniaxial particle models with an aspect ratio equal to $2/3$, if oblate, or $3/2$, if prolate, might also be found optimal in the same sense used for lenses and that moderate biaxial variants of them might form dense disordered packings with further improved characteristics.

ACKNOWLEDGMENTS

The authors are grateful to Charles Maher for his careful reading of the manuscript. G.C. acknowledges the support of the Government of Spain under Grants No. FIS2013-47350-C5-1-R, No. MDM-2014-0377, and No. FIS2017-86007-C3-1-P while S.T. acknowledges the support of the National Science Foundation under Grant No. DMR-1714722.

[1] L. Fejes Tóth, *Regular Figures* (Pergamon, Oxford, 1964).
[2] C. A. Rogers, *Packing and Covering* (Cambridge University Press, Cambridge, 1964).
[3] J. H. Conway and N. J. A. Sloane, *Sphere Packings, Lattices and Groups* (Springer-Verlag, New York, 1999).
[4] C. Zong, *Sphere Packings* (Springer-Verlag, New York, 1999).
[5] P. Brass, W. Moser, and J. Pach, *Research Problems in Discrete Geometry* (Springer-Verlag, New York, 2005).
[6] P. M. Gruber, *Convex and Discrete Geometry* (Springer-Verlag, Berlin, 2007).
[7] G. Grosso and G. Pastori Parravicini, *Solid State Physics* (Academic, San Diego, 2000).

[8] R. Zallen, *The Physics of Amorphous Solids* (Wiley VCH, Weinheim, 2004).

[9] N. H. March and M. P. Tosi, *Introduction to Liquid-State Physics* (World Scientific, Singapore, 2002).

[10] I. N. Levine, *Physical Chemistry* (McGraw-Hill, New York, 2009).

[11] W. D. Callister, *Fundamentals of Materials Science and Engineering* (Wiley, New York, 2001).

[12] G. Rivás and A. P. Minton, Trends Biochem. Sci. **41**, 970 (2016).

[13] J. A. Barker and D. Henderson, Rev. Mod. Phys. **48**, 587 (1976).

[14] *Theory and Simulation of Hard-Sphere Fluids and Related Systems*, edited by A. Mulero (Springer-Verlag, Berlin/Heidelberg, 2008).

[15] G. Parisi and F. Zamponi, Rev. Mod. Phys. **82**, 789 (2010).

[16] S. Torquato and F. H. Stillinger, Rev. Mod. Phys. **82**, 2633 (2010).

[17] A. Santos, Playing with marbles: Structural and thermodynamic properties of hard-sphere systems, in *Proceedings of the 5th Warsaw School of Statistical Physics*, edited by B. Cichocki, M. Napiórkowski, and J. Piaseck (Warsaw University Press, Warsaw, 2014), pp. 203–293; *A Concise Course on the Theory of Classical Liquids* (Springer, New York, 2016).

[18] S. Torquato, J. Chem. Phys. **149**, 020901 (2018).

[19] S. Torquato, *Random Heterogeneous Materials: Microstructure and Macroscopic Properties* (Springer-Verlag, New York, 2002).

[20] J. W. Perram, M. S. Wertheim, J. L. Lebowitz, and G. O. Williams, Chem. Phys. Lett. **105**, 277 (1984); J. W. Perram and M. S. Wertheim, J. Comput. Phys. **58**, 409 (1985).

[21] D. Frenkel, B. M. Mulder, and J. P. Mc Tague, Phys. Rev. Lett. **52**, 287 (1984); D. Frenkel and B. M. Mulder, Mol. Phys. **55**, 1171 (1985).

[22] M. P. Allen and C. P. Mason, Mol. Phys. **86**, 467 (1995); P. J. Camp, C. P. Mason, M. P. Allen, A. A. Khare, and D. A. Kofke, J. Chem. Phys. **105**, 2837 (1996); P. J. Camp and M. P. Allen, *ibid.* **106**, 6681 (1997).

[23] A. Donev, I. Cisse, D. Sachs, E. A. Variano, F. H. Stillinger, R. Connelly, S. Torquato, and P. M. Chaikin, Science **303**, 990 (2004).

[24] A. Donev, F. H. Stillinger, P. M. Chaikin, and S. Torquato, Phys. Rev. Lett. **92**, 255506 (2004).

[25] W. Man, A. Donev, F. H. Stillinger, M. T. Sullivan, W. B. Russel, D. Heeger, S. Inati, S. Torquato, and P. M. Chaikin, Phys. Rev. Lett. **94**, 198001 (2005).

[26] A. Donev, S. Torquato, and F. H. Stillinger, J. Comput. Phys. **202**, 737 (2005); **202**, 765 (2005).

[27] P. M. Chaikin, A. Donev, W. Man, F. H. Stillinger, and S. Torquato, Ind. Eng. Chem. Res. **45**, 6960 (2006); A. Donev, R. Connelly, F. H. Stillinger, and S. Torquato, Phys. Rev. E **75**, 051304 (2007).

[28] P. Pfleiderer and T. Schilling, Phys. Rev. E **75**, 020402(R) (2007); M. Radu, P. Pfleiderer, and T. Schilling, J. Chem. Phys. **131**, 164513 (2009).

[29] G. Odriozola, J. Chem. Phys. **136**, 134505 (2012); G. Bautista-Carvajal, A. Moncho-Jordá, and G. Odriozola, *ibid.* **138**, 064501 (2013).

[30] L. Onsager, Ann. N.Y. Acad. Sci. **51**, 627 (1949).

[31] J. Vielliard-Baron, Mol. Phys. **28**, 809 (1974).

[32] D. W. Rebertus and K. M. Sando, J. Chem. Phys. **67**, 2585 (1977).

[33] M. Hosino, H. Nakano, and H. Kimura, J. Phys. Soc. Jpn. **46**, 1709 (1979); **47**, 740 (1979).

[34] D. Frenkel, J. Phys. Chem. **91**, 4912 (1987); D. Frenkel, H. N. W. Lekkerkerker, and A. Stroobants, Nature (London) **332**, 822 (1988); P. Bolhuis and D. Frenkel, J. Chem. Phys. **106**, 666 (1997).

[35] S. R. Williams and A. P. Philipse, Phys. Rev. E **67**, 051301 (2003).

[36] A. Wouterse, S. R. Williams, and A. P. Philipse, J. Phys.: Condens. Matter **19**, 406215 (2007); A. V. Kyrylyuk, M. A. Haar, L. Rossi, A. Wouterse, and A. P. Philipse, Soft Matter **7**, 1671 (2011); J. Zhao, S. Li, E. Zou, and A. Yu, *ibid.* **8**, 1003 (2012); C. Ferreiro-Córdova and J. S. van Duijneveldt, J. Chem. Eng. Data **59**, 3055 (2014); L. Meng, Y. Jiao, and S. Li, Powder Technol. **292**, 176 (2016).

[37] J. A. C. Veerman and D. Frenkel, Phys. Rev. A **45**, 5632 (1992).

[38] P. D. Duncan, M. Dennison, A. J. Masters, and M. R. Wilson, Phys. Rev. E **79**, 031702 (2009); P. D. Duncan, A. J. Masters, and M. R. Wilson, *ibid.* **84**, 011702 (2011).

[39] Y. Jiao, F. H. Stillinger, and S. Torquato, Phys. Rev. E **79**, 041309 (2009); **81**, 041304 (2010); R. D. Batten, F. H. Stillinger, and S. Torquato, *ibid.* **81**, 061105 (2010).

[40] R. Ni, A. P. Gantapara, J. de Graaf, R. van Roij, and M. Dijkstra, Soft Matter **8**, 8826 (2012).

[41] J. H. Conway and S. Torquato, Proc. Natl. Acad. Sci. USA **103**, 10612 (2006).

[42] E. R. Chen, Discrete Comput. Geom. **40**, 214 (2008).

[43] S. Torquato and Y. Jiao, Nature (London) **460**, 876 (2009); Phys. Rev. E **80**, 041104 (2009).

[44] A. Haji-Akbari, M. Engel, A. S. Keys, X. Zheng, R. G. Petschek, P. Palffy-Muhoray, and S. C. Glotzer, Nature (London) **462**, 773 (2009).

[45] A. Jaoshvili, A. Esakia, M. Porrati, and P. M. Chaikin, Phys. Rev. Lett. **104**, 185501 (2010).

[46] Y. Kallus, V. Elser, and S. Gravel, Discrete Comput. Geom. **44**, 245 (2010).

[47] E. R. Chen, M. Engel, and S. C. Glotzer, Discrete Comput. Geom. **44**, 253 (2010).

[48] S. Torquato and Y. Jiao, Phys. Rev. E **81**, 041310 (2010).

[49] U. Agarwal and F. A. Escobedo, Nat. Mater. **10**, 230 (2011).

[50] Y. Jiao and S. Torquato, J. Chem. Phys. **135**, 151101 (2011); D. Chen, Y. Jiao, and S. Torquato, J. Phys. Chem. B **118**, 7981 (2014).

[51] P. F. Damasceno, M. Engel, and S. C. Glotzer, ACS Nano **6**, 609 (2012); Science **337**, 453 (2012).

[52] G. Cinacchi and S. Torquato, J. Chem. Phys. **143**, 224506 (2015).

[53] G. Cinacchi and S. Torquato, Soft Matter **14**, 8205 (2018).

[54] S. Torquato, T. M. Truskett, and P. G. Debenedetti, Phys. Rev. Lett. **84**, 2064 (2000); This work introduced the concept of MRJ state for hard spheres, including suitable positional and bond-orientational order metrics to quantify the degree of order. The same concept is generalizable to hard nonspherical particles by suitably generalizing those positional and bond-orientational order metrics and adding suitable orientational order metrics.

[55] S. Torquato and F. H. Stillinger, Phys. Rev. E **68**, 041113 (2003).

[56] C. Zachary and S. Torquato, J. Stat. Mech.: Theory Exp. (2009) P12015.
[57] S. Torquato, J. Phys.: Condens. Matter **28**, 414012 (2016).
[58] S. Torquato, Phys. Rep. **745**, 1 (2018).
[59] A. Donev, F. H. Stillinger, and S. Torquato, Phys. Rev. Lett. **95**, 090604 (2005).
[60] C. E. Zachary, Y. Jiao, and S. Torquato, Phys. Rev. Lett. **106**, 178001 (2011); Phys. Rev. E **83**, 051308 (2011); **83**, 051309 (2011).
[61] Y. Jiao and S. Torquato, Phys. Rev. E **84**, 041309 (2011).
[62] One analytic calculation of $\langle v_{\rm exc}\rangle$ for hard convex $\mathsf{D}_{\infty\mathsf{h}}$-symmetric particles including lenses has recently been made by E. Herold, R. Hellmann, and J. Wagner, J. Chem. Phys. **147**, 204102 (2017).
[63] Additional details about this procedure as well as references were provided elsewhere [53]. In the present specific case, the starting dimensionless pressure was equal to 10. It was steadily increased in steps of 5 until a value of 100; in steps of 10 from 100 to 200; in steps of 50 from 200 to 500; in steps of 100 from 500 to 1000. From a dimensionless pressure of 1000, larger values of 1500, 2000, 3000, 4000, 5000, 10 000, 100 000 and 1 000 000 were considered. For any of these values of dimensionless pressure, a run of 2×10^6 Monte Carlo cycles was carried out; during the last 10^6 Monte Carlo cycles, configurations were regularly saved and stored for the successive analysis. The final configuration was then used to start the run at the next higher value of dimensionless pressure. The use of the term "gentle" is motivated by the fact that, by using a similar compression protocol, systems of lenses with, respectively, a less or more pronounced shape anisotropy would form a plastic or liquid crystal [53].
[64] J. G. Kirkwood, J. Chem. Phys. **18**, 380 (1950); W. W. Wood, *ibid.* **20**, 1334 (1952); Z. W. Salsburg and W. W. Wood, *ibid.* **37**, 798 (1962); F. H. Stillinger and Z. W. Salsburg, J. Stat. Phys. **1**, 179 (1969); A. Donev, S. Torquato, and F. H. Stillinger, Phys. Rev. E **71**, 011105 (2005).
[65] T. Boublík, Mol. Phys. **42**, 209 (1980).
[66] In the case of a positionally disordered system with a sufficiently large size, the orientational average over the interparticle vector directions would be complete, hence the $g(r)$ or $\mathcal{S}(k)$ curves smooth, irrespective of whether the system is fluid or solid. Naturally, the curve roughness also depends on the width of the bins, Δr or Δk, of the histograms involved in the numerical calculation of $g(r)$ or $\mathcal{S}(k)$: here, $\Delta r = 0.01\sigma$ and $\Delta k\sigma = 0.1$.
[67] S. Torquato and F. H. Stillinger, Exp. Math. **15**, 307 (2006); A. Scardicchio, F. H. Stillinger, and S. Torquato, J. Math. Phys. **49**, 043301 (2008).
[68] Note that, in the present case,

$$\mathtt{Z} = \langle \mathtt{n}_{\rm c}\rangle = \sum_{\mathtt{n}_{\rm c}\geqslant 0} \mathtt{n}_{\rm c}\Pi(\mathtt{n}_{\rm c}) = 3\varrho\langle v_{\rm exc}\rangle \mathtt{g}(1^+)ds,$$

with $ds = 0.01$.
[69] M. A. Klatt and S. Torquato, Phys. Rev. E **94**, 022152 (2016).
[70] M. A. Klatt and S. Torquato, Phys. Rev. E **97**, 012118 (2018).